Supporting Information

Chen *et al.* 10.1073/pnas.0807752105

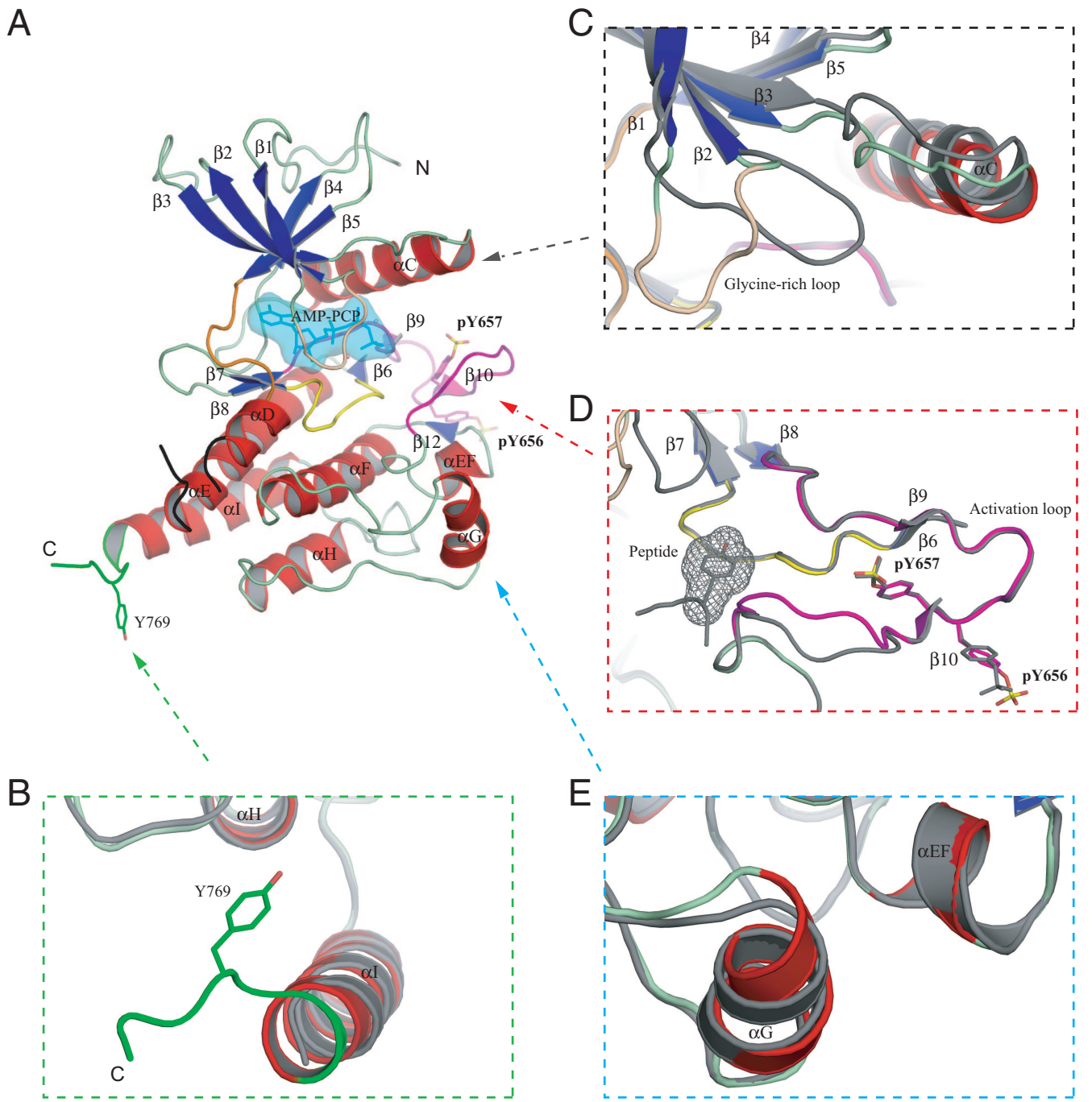

Fig. S1. Crystal structure of the *trans*-phosphorylating kinases structure (3CLY). (*A*) Ribbon diagram of the *trans*-phosphorylating kinases structure. Strands and helices are colored blue and red, respectively. The A-loop, catalytic loop, nucleotide-binding loop, kinase insert and kinase hinge are colored magenta, yellow, wheat, black, and orange, respectively. The extra ordered residues at the C-tail of the *trans*-phosphorylating kinases structure compared with the kinase-peptide structure are colored green. The side chains of the A-loop phosphotyrosines pY656 and pY657 and the C-tail tyrosine Y769 are rendered as sticks. The ATP analogue (in cyan) is shown in stick, and its molecular surface is also shown as a solid semitransparent surface. (*B–E*) Comparison of the *trans*-phosphorylating kinases structure and the kinase-peptide structure (in gray) shows structural deviation at the C-tail (*B*), the αC helix and the nucleotide-binding loop (*C*), the A-loop (*D*) and the αG and αEF helix region (*E*).

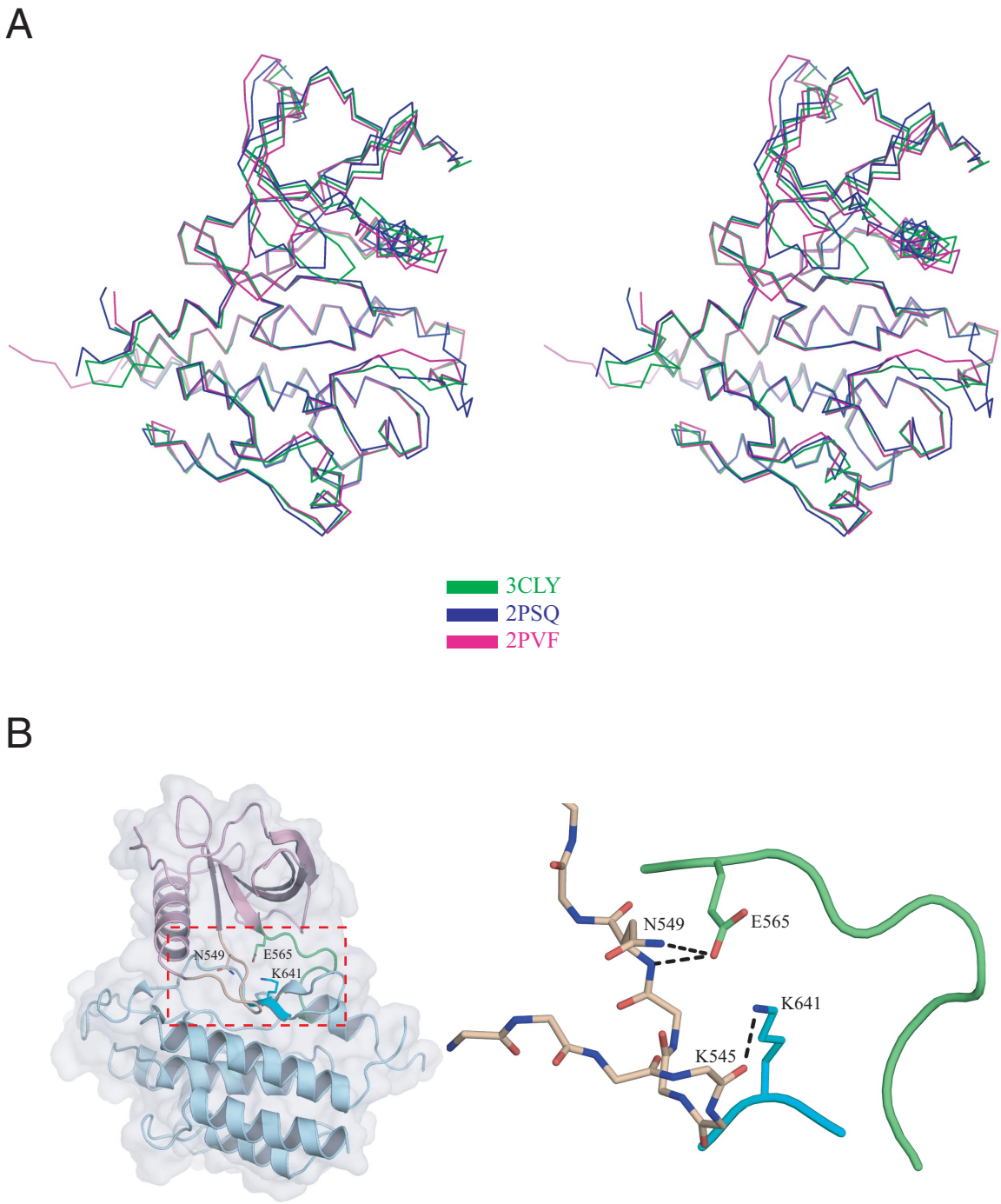

Fig. S2. (*A*) Stereoview of the superimposition of the *trans*-phosphorylating kinases structure (3CLY, in green) with the unphosphorylated wild type kinase structure (2PSQ, in blue) and the kinase-peptide structure (2PVF, in magenta). (*B*) Disengagement of the molecular brake at the hinge of the *trans*-phosphorylating kinases structure.

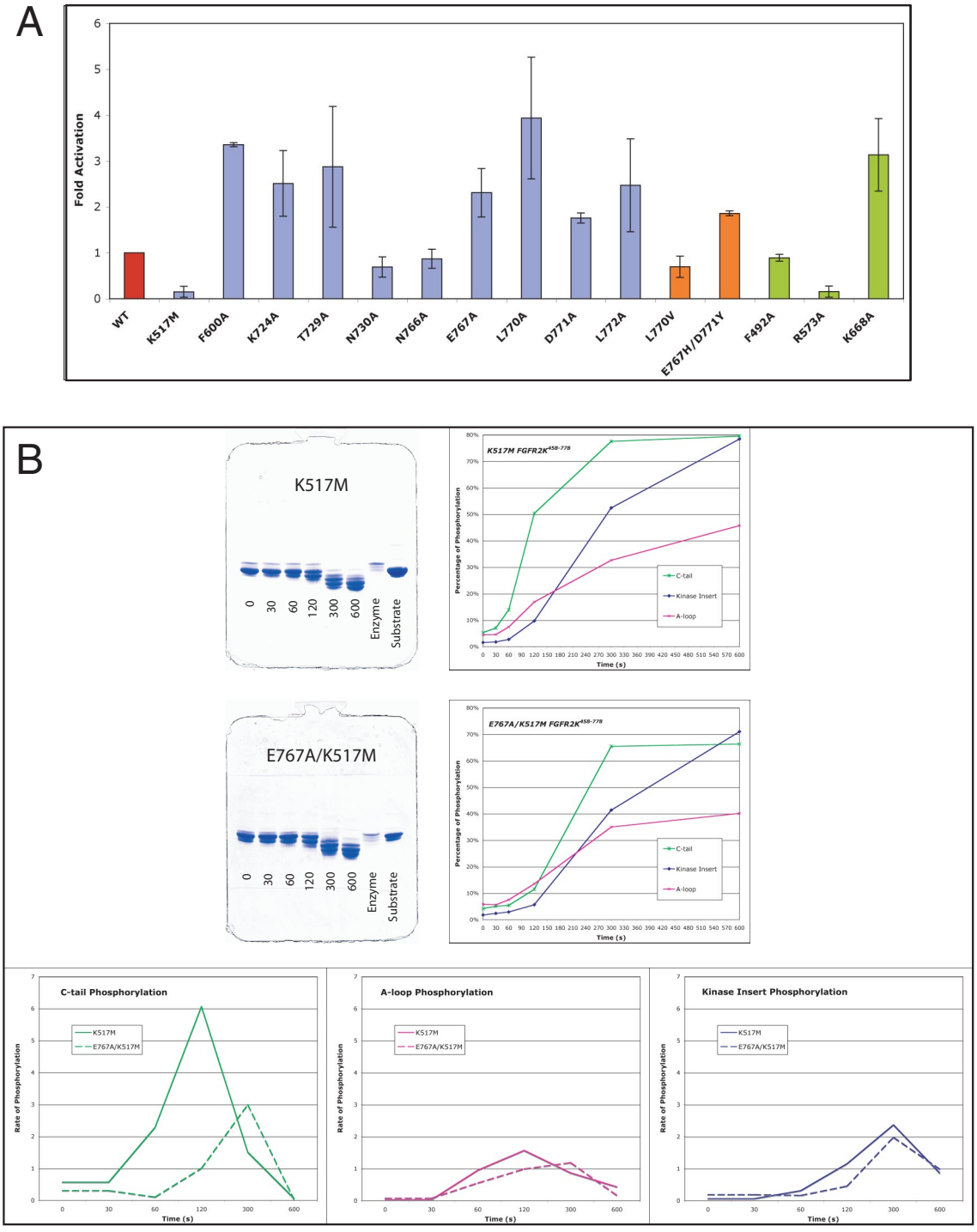

Fig. S3. Effects of enzyme-substrate interface mutations on kinase activity and phosphorylation of different tyrosine phosphorylation sites. (*A*) Autophosphorylation assays: unphosphorylated wild type or mutant FGFR2K$^{458–778}$s were incubated with 1 mM ATP, and autophosphorylation rates were determined using a continuous spectrophotometric assay. WT, C-lobe, N-lobe and pathogenic mutant kinases are colored red, light blue, green and orange, respectively. (*B*) Comparison of the time course of phosphorylation by enzyme-acting kinase of the different tyrosine sites at the C-tail, the A-loop and the kinase insert in WT kinase substrate and E767A mutant kinase substrate shows that the E767A mutation impair the Y769 phosphorylation but has little effects on phosphorylation of tyrosines in the A-loop and the kinase insert. Ion counts of the phosphopeptide and its unphosphorylated version are used to estimate the percentage of phosphorylation and the rate of phosphorylation of the different sites in the 2 substrate-acting kinases. Accompanying native gels also show the differences in the progress of tyrosine phosphorylations in real time.

Fig. S4. Structure-based sequence alignment of the αI helix region of RTKs. Note that the αI helix in the *trans*-phosphorylating kinases structure (blue box) is elongated by 3 residues relative to that in the kinase-peptide structure (red box). The αI helices of FGFR1 (PDB entry 1FGK), Ret (PDB entry 2IVT), Tek/Tie2 (PDB entry 1FVR), Met (PDB entry 1R1W), and c-Kit (PDB entry 1T45) are also highlighted with a red box. Several RTKs possess known tyrosine autophosphorylation sites (colored in green) at the homologous position to Y769 of FGFR2. PDGFR has also a potential tyrosine phosphorylation site at this location (orange).

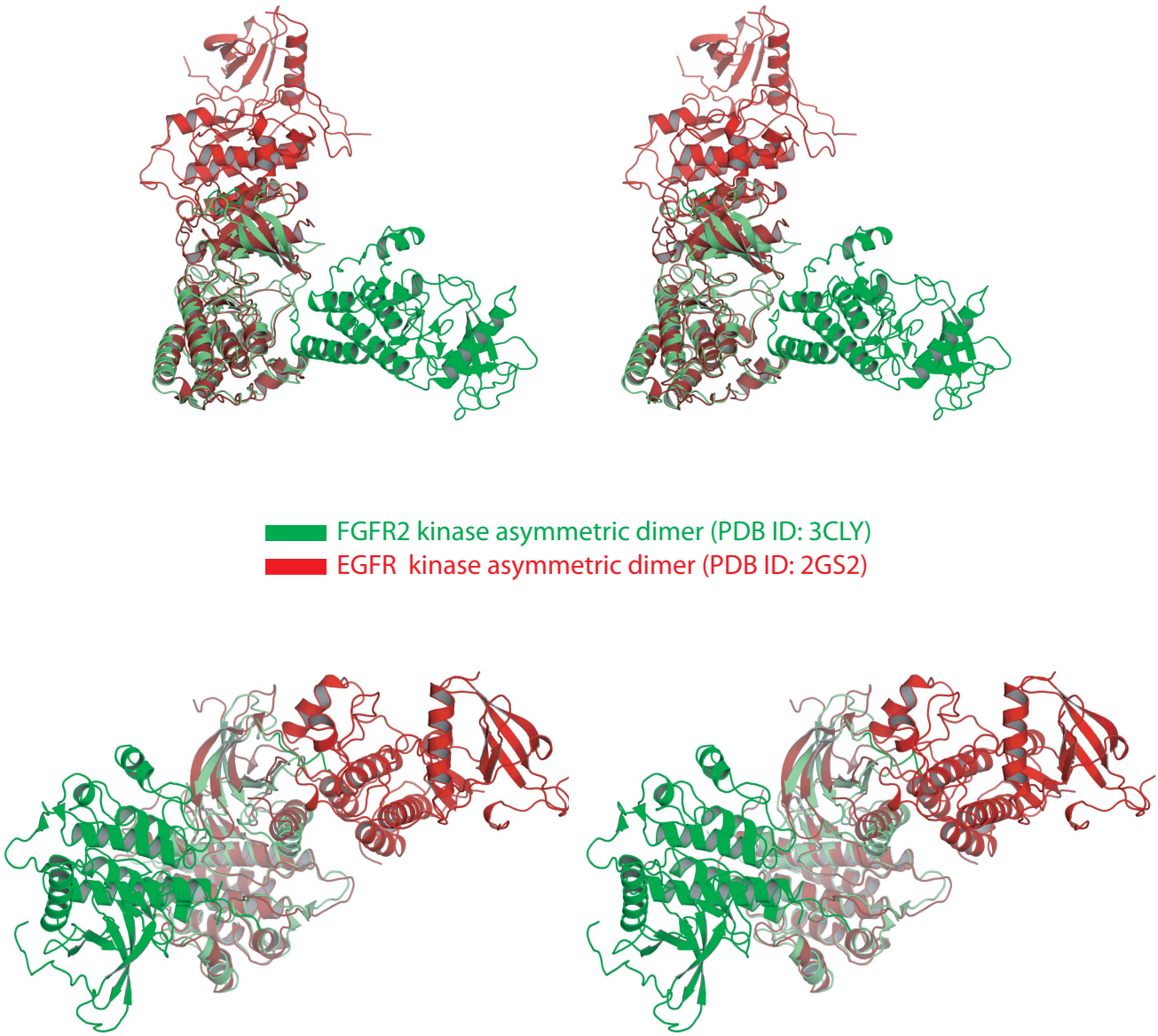

Fig. S5. The topology of the FGFR2K *trans*-phosphorylating asymmetric dimer is different from that of the EGFRK activating asymmetric dimer. Stereo views of FGFR2K enzyme-acting kinase:substrate-acting kinase dimer (PDB entry 3CLY, in green) and the EGFRK dimer after superimposition of the enzyme-acting kinase from 3CLY onto 1 EGFRK monomer (PDB entry 2GS2, in red). The asymmetric EGFRK dimer depicts kinase activation by homodimerization whereas the asymmetric FGFR2K dimer depicts *trans*-phosphorylation after kinase activation.

Table S1. Data collection and refinement statistics

Construct	Phosphorylated FGFR2K$^{458–778}$
Data Collection	
Resolution, Å	50–2.0 (2.07–2.00)
Space group	$P2_12_12_1$
Unit cell parameters	
a, Å	55.437
b, Å	68.462
c, Å	85.711
$\alpha = \beta = \gamma$, °	90
Content of the asymmetric unit	1
No. of measured reflections	272,640
No. of unique reflections	23,066 (2,219)
Data redundancy	11.8 (8.6)
Data completeness, %	99.5 (97.6)
R_{sym}, %	6.0 (15.7)
I/sig	30.0
Refinement	
R factor/R_{free}	21.6/24.7
No. of protein atoms	2267
No. of nonprotein/solvent atoms	33
No. of solvent molecules	107
rmsd	
Bond length, Å	0.005
Bond angle, °	1.4
B factor, Å^2	1.4
PDB ID	3CLY

Numbers in parenthesis refer to the highest resolution shell. $R_{sym} = \Sigma|I - \langle I\rangle|/\Sigma I$, where *I* is the observed intensity of a reflection, and $\langle I\rangle$ is the average intensity of all the symmetry related reflections.